Seaweed as Novel Biofiller in Polypropylene Composites

Lixing Luan,[1,2] Wei Wu,[1] Manfred H. Wagner,[2] Marco Mueller[2]

[1]*School of Materials Science and Engineering, East China University of Science and Technology, Shanghai 200237, China*
[2]*Polymer Engineering/Polymer Physics, Berlin Institute of Technology (TU Berlin), Berlin 10623, Germany*

Received 12 January 2010; accepted 14 March 2010
DOI 10.1002/app.32462
Published online 27 May 2010 in Wiley InterScience (www.interscience.wiley.com).

ABSTRACT: Based on former exploratory research, we used seaweed (SW) fiber as a novel biofiller for the production of polypropylene (PP) biocomposites. Maleic anhydride-grafted polypropylene (MAPP) and a CNT masterbatch (CESA) were applied as compatibilizers. Mechanical properties, crystallization behavior, dynamic mechanical performance as well as interfacial morphology were characterized. SW fiber was successfully incorporated in the PP matrix in terms of mechanical reinforcement. Accelerated crystallization process of PP matrix was observed. DMA results also indicated the favorable adhesion between SW fiber and PP matrix, which could be confirmed by SEM characterization. The effect and efficiency of MAPP and CESA as compatibilizers were evaluated. Moreover, potential flame retardancy of SW fibers for PP matrix was observed, and satisfying results warrant further investigations. © 2010 Wiley Periodicals, Inc. J Appl Polym Sci 118: 997–1005, 2010

Key words: PP/SW biocomposites; mechanical properties; thermal dynamic behavior; flame retardancy

INTRODUCTION

Polymer/natural fiber biocomposites have recently drawn great attentions in fundamental research and industrial applications for their ecological and economic advantages. Besides environmental concerns, natural fiber reinforced polymer biocomposites provide a unique combination of high performance, great versatility, and processing advantages at favorable costs. Natural lignocellulosic fibers are renewable, completely or partially recyclable and biodegradable; flax, cotton, hemp as well as wood fiber are applied as biofillers into polymeric matrices.[1–4] Their significant weight saving, low cost and other advantages promote natural fibers as ideal alternative fillers to glass and carbon fibers. Natural fiber biocomposites have already appeared in industrial scale as furniture, household appliances, and as automotive materials.[5]

The biggest drawback of lignocellulosic fibers is their hydrophilic nature. The high polar surface of those fibers leads to weak interactions with nonpolar polymeric matrices, such as polyethylene (PE) and polypropylene (PP). Many methods were proposed for improving adhesion between natural fibers and polymeric matrix: surface modification, graft polymerization, UV radiation and coupling agents such as silane, alkali, maleic anhydride-grafted copolymers. Esterification bonding by maleic copolymer coupling agents was reported to be efficient in overcoming the incompatibility between natural fibers and polymeric matrices.[6,7] Moreover, the aggregation tendency and poor resistance to moisture of natural fibers must be considered; low degradation temperature (normally $<200^{\circ}C$) of most natural fibers also limits their processing efficiency with thermoplastics under higher temperature and shear stress.[8,9]

Satisfying mechanical properties of different polymer/natural fiber biocomposites have been reported. Natural fibers have successfully enhanced polymeric matrices with and even without compatibilizers at different natural fiber loadings.[8,10–12] Thermal properties of lignocellulosic biocomposites are also of great importance. Remarkable promotion of crystallinity of polymer matrix by natural fibers was reported. This phenomenon may be attributed to two aspects: one is transcrystallinity, with heterogeneous nucleation generating α-layer from the fiber surface, and cylindrical crystallization may occur by self-nucleation. Another reason may lie in homogenous nucleation which generates ß-crystals from α-crystals.[13] Certain treatments can avoid the formation of transcrystallinity or provide active sites on fiber surface to form transcrystalline regions.[14] It has also been proposed that because of the interaction of the polymeric chains and the fiber surface, transcrystallinity can improve the adhesion between natural fiber and polymer.[15]

Flame resistance is yet another important criterion for the final application of composites. It is obvious

Correspondence to: M. H. Wagner (manfred.wagner@tu-berlin.de).

TABLE I
Minor Content of Seaweed Fibers

Ingredients	Content (wt %)	Ingredients	Content (mg/kg DM)
Nitrogen	0.05	Aqua regia zinc	142
Phosphate	0.08	Aqua regia copper	9.38
Potash	0.20	Aqua regia iron	476
Aqua regia calcium	0.56	Auqa regia manganese	42.13
Aqua regia magnesium	1.04	Aqua regia sulphur	21900
Aqua regia sodium	7.54	Boron	363

that most polymers are sensitive to flame, but a certain level of flame resistance is required for application safety. Because of environmental concerns, use of flame retardants has moved from halogenated compounds to phosphorous compounds and more recently to inorganic compounds, such as metallic hydroxide additives.[16–18] Only few publications have reported the inherent flame retardancy of certain natural fibers in polymeric matrices.[19]

In earlier work, we have reported an exploratory investigation using seaweed fiber as novel natural reinforcing filler for PP matrix, and achieved certain mechanical enhancements.[20] In this work, we undertake an indepth research into the use of seaweed fiber as biofiller by preparing a series of polypropylene/seaweed (PP/SW) biocomposites. Also, in this work, we study maleic anhydride-grafted polypropylene (MAPP) and a carbon nanotube (CNT) masterbatch (CESA) as compatibilizers. Mechanical properties, crystallization behavior, dynamic mechanical performance, and interfacial morphology of PP/SW composites were systematically investigated, while unexpected flame retardancy effects of SW fiber for PP were also observed.

METHODS

Materials

PP was supplied by Sabic (PP 579S; density = 0.905g/cm^3; MFI = 47 g/10 min). Seaweed fiber (SW) was obtained from Natural Garden (Birmingham, GB). The raw seaweed is *Ascophyllum nodosum* harvested from the Shetland Isles, the minor contents are listed in Table I. Maleic anhydride polypropylene (MAPP) was obtained from Aldrich (MAPP; MA% = 8–10 wt %). Masterbatch CESA (CESA®-conductive CNT OC90025520) was supplied by Clariant; the polymer matrix of this masterbatch is a suitable lubricant for the use with PP.

Pretreatments

Seaweed fiber is hydrophilic and absorbs moisture like other cellulosic fibers. The moisture content is between 5–10 wt % as received, which may lead to dimensional variations in composites and reduction in final properties, thus the raw fiber was first dried at 60°C for 24 h. The dimensions of the fibrous material could also be a dominating factor for fiber distribution and orientation. The as-received SW pellets are about 2 mm in diameter, and were then granulated by a twin rotary miller (Cutting Milling A11, IKA) to a dimension of ~0.1 mm. The granulated SW fibers were dried again at 60°C for 48 h before compounding. PP, MAPP, and CESA were used after drying at 60°C for 24 h before compounding.

Composites and preparation

The composition of PP/SW biocomposites prepared in this work is listed in Table II. PP, SW, MAPP, and CESA were precisely weighted, and the content of MAPP was fixed to the SW content. Raw materials were well mixed by a Batch Blender (Testing GmbH, Germany) at 285 rpm for 20 mins. The compounding was done by use of an extruder (L/D = 20, Collin GmbH, Germany) under 175/180/185/180°C, Screw rotation speed 60 rpm. The extrudates were dried at 60°C for 24 h, and then granulated to ~ 2 mm by a grinding mill (Herbold GmbH, Germany).

Dumbbell-shaped bars (ASTM 527) for mechanical testing were prepared by injection molding (L/D = 22.3 BOY 30A, Germany), under 175/180/185/180°C, screw rotation speed 60 rpm, mold temperature 60°C, cooling time 45 sec, injection and molding pressure 60 bars.

TABLE II
Compositions of PP/SW Biocomposites

Sample	PP (wt %)	SW (wt %)	MAPP (wt %)	CESA (wt %)
PP	100			
SW20	80	20		
SW30	70	30		
SW40	60	40		
SW20MAPP	80	20	2.5	
SW30MAPP	70	30	2.5	
SW40MAPP	60	40	2.5	
SW20CESA	80	20		5
SW30CESA	70	30		5
SW40CESA	60	40		5

Specimens for Dynamic Mechanical Analysis (DMA) of size 60 mm × 10 mm × 2 mm were shaped from the testing bars.

Differential Scanning Calorimetry (DSC) samples were sliced from testing bars with 50 μm thickness by Cut 4055 (MicroTec GmbH, Germany).

Test plates for Cone Calorimetric Analysis of dimension 100 mm × 100 mm × 8 mm were prepared by hot compression at 200°C and 10 bars for 20 mins.

Mechanical characterization

Testing bars were conditioned at 23°C, 50% humidity before characterization (ASTM D618). The Shore hardness (Shore D) was measured with a Zwick 3150 (Zwick GmbH, Germany) according to ASTM D2240. Tensile properties were tested by use of a Zwick Z010 (Zwick GmbH, Germany) testing machine with a load cell capacity of 10KN at a cross-head speed of 50 mm/min (ASTM D527). Flexural tests (ASTM 279) were carried out by three-point bending test method with cross-head speed at 1 mm/min on a Zwick 2201 (Zwick GmbH, Germany). At least five specimens were measured for each sample, mean values and standard deviations were calculated.

Differential scanning calorimetry analysis

Differential scanning calorimetry (DSC) analysis was performed on a DSC 822 (Mettler Toledo) under nitrogen atmosphere. Temperature was raised by 10 K/min from ambient temperature to 250°C, isothermal for 4 min to eliminate previous thermal history, and cooled down to 50°C at 10 K/min. The samples were then reheated to 250°C, isothermal for 3 min and cooled down to 50°C by 10 K/min to trace thermal behavior.

Dynamic mechanical analysis

DMA was performed on a DMA 2980 (TA Instruments). The samples were scanned under dual cantilever mode over a temperature range from –50°C to 150°C with a heating rate of 3 K/min, oscillation frequency 1 Hz and strain amplitude 1% (within the linear viscoelastic region). E', E'' and tan δ (loss factor) were recorded.

Scanning electron microscopy characterization

Scanning electron microscopy (SEM) was taken on a S-520 (Hitachi, Japan) under 20 kV accelerating voltage to analyze the fracture morphology of PP/SW biocomposites. The mechanical test bar was fractured within liquid nitrogen, and the fracture surface was coated with gold before characterization.

Cone calorimetric analysis

The fire behavior of PP/SW biocomposites was explored by Cone Calorimetric Analysis (Fire Testing Technology, UK) according to ISO 5660. Only neat PP and SW30 were characterized for the fundamental exploration in this article, and at least five samples were evaluated. Further systematic characterizations of flame retardancy are under investigation and will be reported in later work.

RESULTS AND DISCUSSIONS

Mechanical Characterizations

Tensile and flexural properties as well as hardness (Shore D) of PP/SW biocomposites were evaluated and elastic modulus, tensile strength at break, flexural modulus and flexural strength are reported in Figure 1 and Table III.

All samples showed similar hardness [Fig. 1(a)], which implies good adhesion between matrix and fiber as well as the appropriateness of the processing parameters adopted in this article. The surface hardness reflects the efficiency of the reinforcement of matrix and matrix surface by the filler.[21] Incorporation of raw SW into the matrix maintains the hardness of neat PP, and MAPP leads to an increase of this material parameter, while adding CESA brings about little difference for the value of surface hardness. This indicates that raw SW fiber is capable of mechanical reinforcement of the PP matrix, and MAPP could generate further improvement.

As expected, mechanical results indicate a satisfying maintenance of mechanical strength by adding SW within the loading range of 20–40 wt%. A slight decline in tensile strength is observed for raw SW samples [Fig. 1(b)], while CESA and MAPP successfully improved the tensile property. It is generally understood that the uniformity of fibers would increase the strength by lateral fiber bonds, while without proper treatment, most lignocellulosic fibers are not beneficial for mechanical enforcement of polyolefins. Theoretically, an enhancement of composite material properties is expected by incorporating a higher volume fraction of filler, and by creating efficient stress-transfer at the matrix-fiber interfaces. The stress transfer from the matrix to the fiber depends on fiber-matrix and fiber-fiber interactions.[22]

The mechanism for MAPP was generally accepted as eliminating weak boundary layers by chemical bondings at the matrix-fiber interface.[6,8,12] It is worth noting that CESA also shows a high compatibilizing

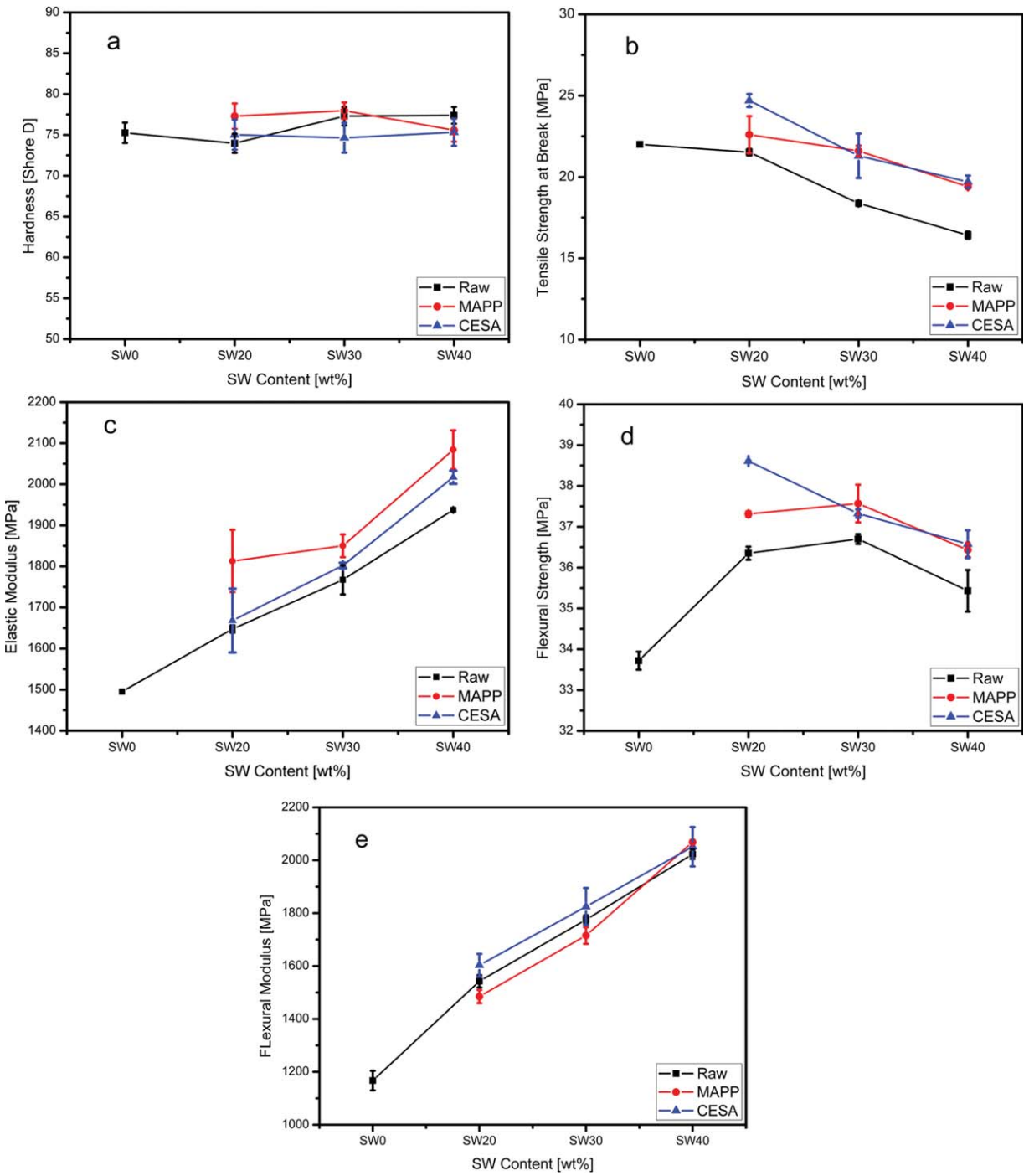

Figure 1 Mechanical properties of PP/SW biocomposite: (a) Shore D hardness; (b) Tensile strength at break; (c) Elastic modulus; (d) flexural strength at break; (e) flexural modulus. [Color figure can be viewed in the online issue, which is available at www.interscience.wiley.com.]

efficiency. This phenomenon could be explained by CESA successfully improving the wettability of SW fiber by PP matrix, and thereby creating a deformable, tough and flexible layer. This will be further confirmed by other material characterizations.

Elastic modulus [Fig. 1(c)], flexural strength [Fig. 1(d)] and flexural modulus [Fig. 1(e)] were all noticeably improved by SW fiber addition, both with and without compatibilizers (Table III). Raw SW generates up to 30% increase in elastic modulus and 70% increase in flexural modulus, and the values increase with SW loadings. This is because SW fibers are ductile, and the micro fibrils have a spiral orientation with respect to the fiber axis. The use of MAPP and CESA lead to similar extents of further improvement: 40% for elastic modulus and 75% for flexural modulus. The spiral orientation of SW fiber is responsible for the natural elasticity of the

TABLE III
Mechanical Properties of PP/SW Biocomposites

Sample	Shore D hardness	Elastic modulus (MPa)	Flexural modulus (MPa)
PP	75 (1)[a]	1495 (10)	1167 (37)
SW20	74 (1)	1648 (9)	1542 (23)
SW30	77 (1)	1767 (36)	1775 (18)
SW40	77 (1)	1934 (3)	2023 (18)
SW20MAPP	78 (2)	1813 (76)	1485 (25)
SW30MAPP	78 (1)	1850 (28)	1715 (31)
SW40MAPP	76 (1)	2084 (47)	2069 (8)
SW20CESA	75 (2)	1668 (78)	1603 (43)
SW30CESA	75 (2)	1802 (7)	1825 (70)
SW40CESA	75 (2)	2017 (16)	2051 (74)

[a] Represents standard deviation.

SW fiber, and the impregnation of the SW fiber improved the elastic modulus and the flexural properties of the PP matrix.

DSC analysis

The thermal behavior of PP/SW biocomposites were analyzed by DSC. T_p (peak temperature of crystallization) and T_c (onset temperature of crystallization) were recorded during the cooling process, while T_m (melting temperature) and ΔH_m (heat of fusion) were recorded during the heating process. Subsequently the degree of crystallization, X_c, was calculated. The corrected quantities $\Delta H_m'$ and X_c' were obtained by accounting for the SW contents according to

$$\Delta H_m' = \frac{\Delta H_m}{1-\alpha} \quad (1)$$

$$X_c' = \frac{\Delta H_m}{(1-\alpha)\Delta H_0} \quad (2)$$

α stands for the SW content in the PP matrix, and a value of $\Delta H_0 = 207.1$ J/g was used for neat PP.[23]

Figure 2 presents the heating curves obtained by DSC for several SW samples. The melting points of MAPP and CESA could not be resolved due to their low concentration. Little effect of SW fiber content on T_m of the PP matrix is found. However, while

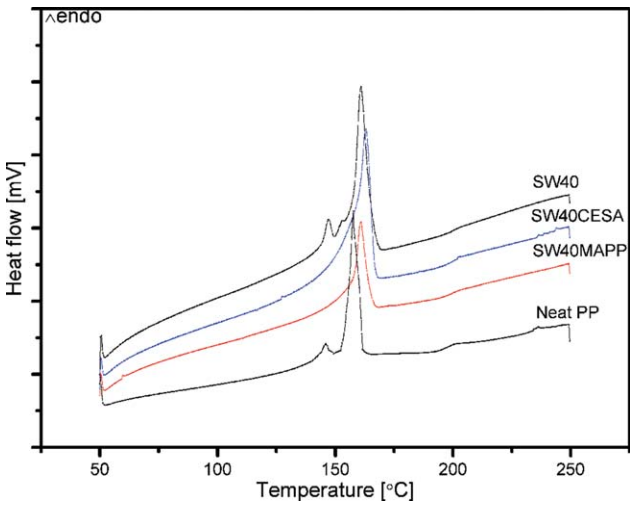

Figure 2 Heating curves of SW40 series PP/SW biocomposites. [Color figure can be viewed in the online issue, which is available at www.interscience.wiley.com.]

two melting points were observed for raw SW40, only one melting point was traced for SW40MAPP and SW40CESA. As reported, the DSC curves for neat PP revealed two melting points representing α- and ß-form crystals, which are consistent with the distinct lamellar thickness and thermal stability of the two crystal forms.[24,25] The absence of the melting peak at the lower temperature may be attributed to the enhanced dispersion of SW fiber and the enhanced adhesion between matrix and fiber that influences the crystallization process and eliminates the difference between the two crystal forms. Moreover, the hypothesis of co-crystallization of PP and MAPP was already proposed, showing the existence of MAPP within the spherulitic structure of PP and the formation of isomorphic crystals in composites,[26] which could also explain the single peak behavior. The crystallization parameters obtained for PP/SW biocomposites are listed in Table IV.

Heat of fusion (ΔH_m) is an important parameter for crystallization. For composites, positive fillers would raise the value of ΔH_m, negative fillers cause a decrease of ΔH_m, while inert fillers lead to

TABLE IV
Nonisothermal Crystallization Parameters in Heating Process of PP/SW Biocomposites

Sample	T_m (°C)	ΔH_m (J/g)	$\Delta H'_m$ (J/g)	X_c (%)	X_c' (%)
PP	158	64.61	64.61	31.20	31.20
SW20	160	72.85	91.06	35.18	43.98
SW30	160	58.82	84.03	28.40	40.57
SW40	161	31.81	53.07	15.36	25.60
SW20MAPP	160	61.61	77.01	29.75	37.19
SW30MAPP	160	64.34	91.91	31.07	44.39
SW40MAPP	161	62.79	104.65	30.32	50.53
SW20CESA	163	56.97	71.21	27.51	34.39
SW30CESA	162	57.67	82.39	27.85	39.79
SW40CESA	163	54.71	91.18	26.42	44.03

TABLE V
Nonisothermal Crystallization Parameters in Cooling Process of PP/SW Biocomposites

Sample	T_p (°C)	T_c (°C)	T_c–T_p (°C)
PP	109	130	21
SW20	120	131	11
SW30	119	131	12
SW40	121	135	14
SW20MAPP	122	135	13
SW30MAPP	121	134	13
SW40MAPP	122	135	13
SW20CESA	126	138	12
SW30CESA	126	139	13
SW40CESA	126	137	11

marginal effects of ΔH_m. Because of the amorphous nature of SW fiber, the $\Delta H_m'$ values are of interest. The value of $\Delta H_m'$ dropped with SW fiber loading without compatibilizer: this decline signifies the negative influence on crystallinity by the interaction between natural fiber and matrix, as raw SW fiber may obstruct the mobility of the PP chain and prevent the macromolecular segments from obtaining ordered alignment in the crystal lattice. While adding MAPP and CESA demonstrate a promoting trend of crystallinity, this fact confirms the better matrix-fiber interfacial adhesion. In other words, MAPP and CESA transform the SW fiber from being negative filler into being positive filler for PP matrix.

Also, the degree of crystallization (X_c') presents distinctive trends for PP/SW biocomposites with and without compatibilizers. Increasing raw SW fiber loadings reduced the X_c', while with MAPP and CESA, SW fiber contents promoted the degree of crystallization for PP/SW biocomposites. Furthermore, the value of [T_c–T_p] dropped from 20 K for neat PP to about 13 K for PP/SW biocomposites (Table V), which implies that SW fiber greatly accelerated the crystallization process of PP matrix. This effect is due to a nucleation effect: SW fibers act as sites for heterogeneous nucleation that induce the crystallization of the PP matrix.

DMA analysis

The storage modulus (E') of PP/SW biocomposites show similar shapes as neat PP, while a prominent increase in E' can be observed [Fig. 3(a)]. E' drops dramatically in the vicinity of the glass transition temperature T_g, which indicates a glass-rubber transition. Also, much higher loss moduli (E'') were recorded for PP/SW biocomposites as compared to neat PP [Fig. 3(b)]. Two major transitions were traced within the testing temperature range, the α and β-transition. The glass transition temperature was recorded from tan δ (damping peak), and transition temperatures from DMA tests are listed in Table VI.

The β-transition is related to the glass-rubber transition, and is a sign of the molecular motions associated with unrestricted amorphous PP.[27,28] For PP/SW biocomposites, we found that T_g declined with SW fiber loadings. MAPP induced a slight increase, and the addition of CESA leads to a remarkable decrease of T_g.

Many works demonstrated a clear drop of T_g with the addition of natural fibers. For raw SW samples (SW20, SW30, SW40), the decrease of T_g may be caused by the reduced degree of crystallization. Another explanation could be that during compounding, some of the SW fiber surface may be sheared off from the fiber, which consists of lignin, cellulose, and other surface extractives that inherently exist in the fiber. Therefore, it might be possible that the sheared-off material was responsible for the decrease of T_g values.

It is expected that the plasticization effect of coupling agent improves the mobility of the polymer

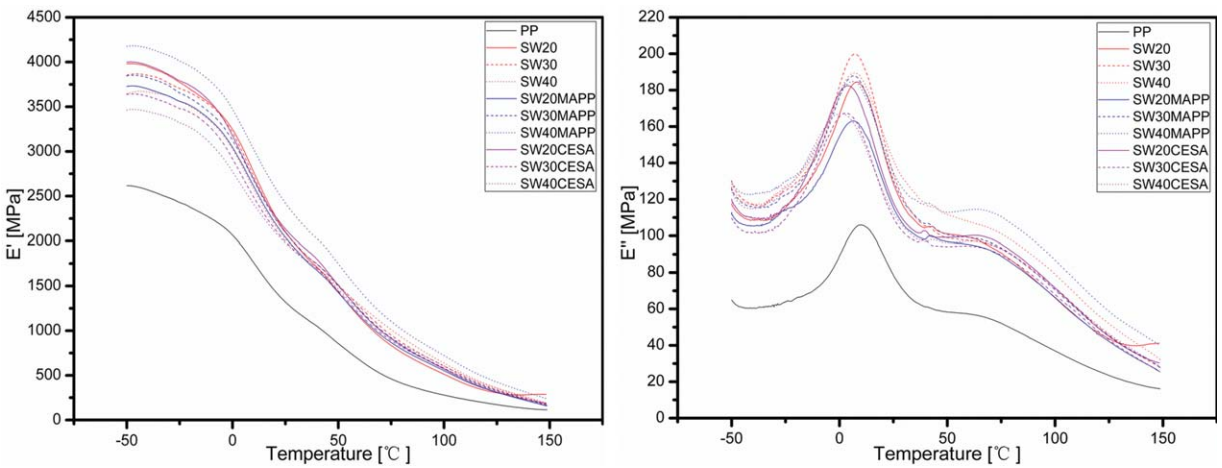

Figure 3 E' (a) and E'' (b) of PP/SW biocomposites from DMA. [Color figure can be viewed in the online issue, which is available at www.interscience.wiley.com.]

TABLE VI
Transition Temperatures of PP/SW BIOCOMPOSITES from DMA

Sample	Glass transition (°C)	β-transition (°C)	α- transition (°C)
PP	16.1	10	53
SW20	14.7	7	63
SW30	14.1	7	72
SW40	15.5	7	73
SW20MAPP	14.4	9	72
SW30MAPP	13.7	8	73
SW40MAPP	13.1	7	74
SW20CESA	9.5	3	68
SW30CESA	9.3	3	68
SW40CESA	8.9	1	69

backbones and thus eventually leads to a decrease of T_g.[29] However, similar to the reported findings for PP/Wood biocomposites,[30] we see only a minor change of T_g in the case of MAPP addition. However, a remarkable decrease of T_g was induced by CESA. This may be attributed to the high efficiency of CESA in improving the wettability of SW fiber by the PP matrix. With better penetration of SW fiber by the PP matrix, the chain mobility is reduced and a drop of T_g is found.

The second transition seen in the DMA curves is the α-transition. As reported in Table VI, all α-transition temperatures for PP/SW biocomposites are much higher than for neat PP. This is in agreement with the fact that rigid SW fibers introduce defects into the crystalline phase of the PP matrix. By smoothing interfaces and improving the wettability of SW fiber by the PP matrix, the addition of CESA lowered the α-transition temperature. The temperature and intensity of the α-transition is related to the relaxation of restricted amorphous PP chains in the crystalline phase, and represents the degree of defects in the crystalline phase. The intensity of the α-transition in comparison with neat PP indicates the number of those defects.[27] The E″ curve for the SW40 series (SW40, SW40MAPP, SW40CESA) is shown in Figure 4. Raw SW fibers lead to a higher intensity of the α-transition as compared with neat PP. The random covalent bonds created by adding MAPP increase the intensity further. In other words, the plasticization effect also leads to a higher proportion of disordered crystalline structures. As expected, the smallest intensity of the α-transition was found for SW40CESA, which is in consistent with the smoothened interface between SW fiber and PP matrix.

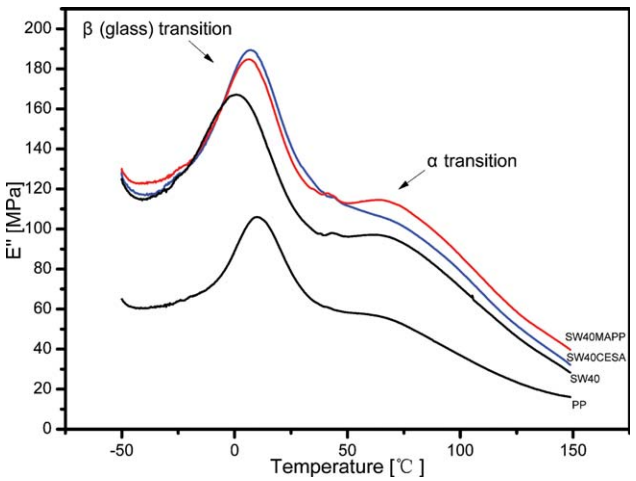

Figure 4 *E″* of SW40 series PP/SW biocomposites from DMA. [Color figure can be viewed in the online issue, which is available at www.interscience.wiley.com.]

Scanning electron microscopy

The interfacial morphology of PP/SW biocomposites were examined by SEM characterization. In agreement with our former work, the addition of raw SW fiber induced disordered microstructures within the PP matrix, as can be found in the SW20 sample (Fig. 5). MAPP successfully improved the interfacial adhesion, the "snapped" SW fibers can easily be observed on the fracture surface of the SW20MAPP sample. The interfacial morphology was transferred

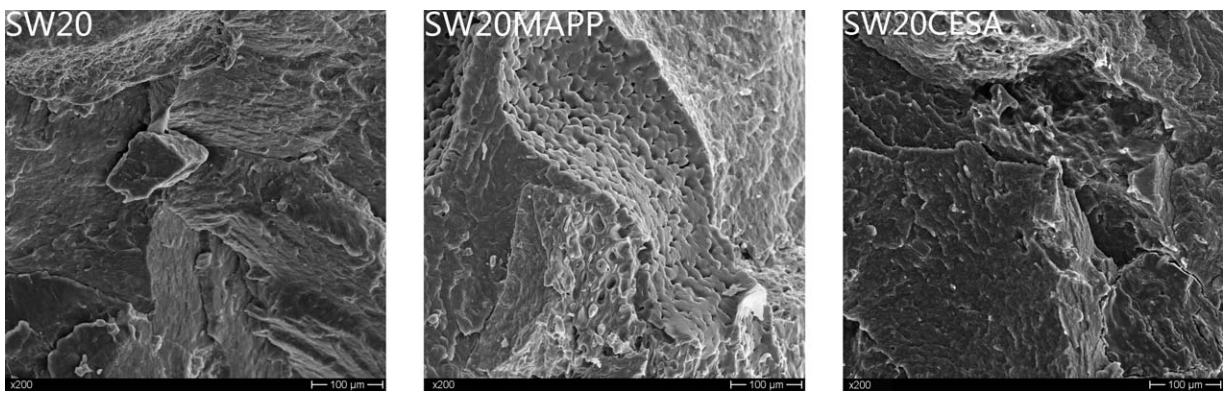

Figure 5 Morphology of SW20 series biocomposites by SEM (from left to right: SW20, SW20MAPP, SW20CESA).

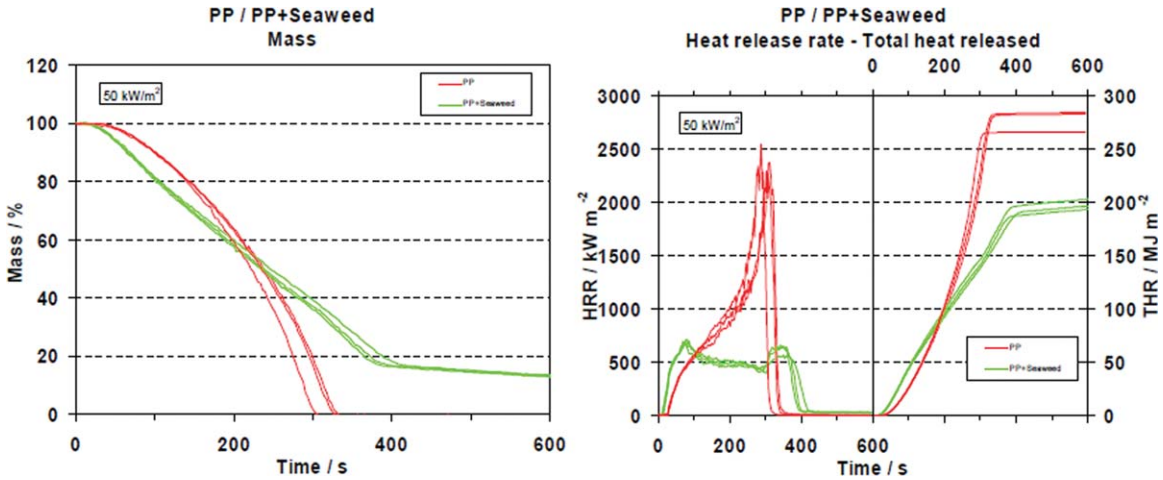

Figure 6 Curves for HRR, THR (a) and Mass Loss (b) from cone calorimetric tests. [Color figure can be viewed in the online issue, which is available at www.interscience.wiley.com.]

into a smooth, fuzzy structure by adding CESA, which confirms the improved wettability of SW fibers by PP matrix.

Fire retardant behavior of SW fibre

First exploratory experiments on the fire behavior of PP/SW biocomposites were made. Surprisingly, remarkable flame retardancy was observed for PP/SW biocomposites as illustrated in Figure 6 and Table VII. The results of neat PP showed the typical high peak heat release rate (PHRR) and total heat release (THR). After addition of SW fibers, a remarkable reduction (30.5% for THR and 71% for PHRR) in THR and PHRR was observed. Further, hardly any residue was obtained for the neat PP plate after combustion, while for the SW30 sample, the residual mass was 16.1% (Fig. 7). Based on the "two-peak" shape of the heat release rate (HRR) curve and the distribution of residue for SW30, it is reasonable to assume that the SW fiber formed char protection under the heat flux, thereby protecting the PP matrix from instant combustion.

A reduction in the time to ignition (TTI) for SW30 compared with neat PP is observed, which is in agreement with the "candle wick" theory proposed for the flammability of polymer/natural fiber composites.[15] Under certain circumstances, a lower TTI value could indicate a higher risk in application of PP/SW biocomposites, which might hamper its potential use as high fire-resistance material. Further work is needed for investigating the early burning stage of PP/SW biocomposites.

CONCLUSIONS

Based on our former exploratory research work on seaweed as novel biofiller, the distinctive mechanical and thermal performance of PP/SW biocomposites was systematically evaluated in this work. With proper compatibilizers, the addition of SW fiber could maintain and slightly enforce the mechanical properties of PP matrix. Based on DSC, DMA, and SEM characterizations, the crystallization process of the PP matrix was accelerated by the addition of SW fiber. MAPP and CESA successfully transformed SW fiber from a negative filler into a positive filler for the PP matrix. MAPP improved the interfacial adhesion by covalent interactions, while CESA showed an even higher efficiency in mechanical and thermal reinforcement by improving the wettability of SW fiber by the PP matrix. Furthermore, first results on the effect of seaweed on the flame retardancy of PP/SW biocomposites demonstrate an important potential for the use of seaweed as flame retardant.

TABLE VII
Parameters from Cone Calorimetric Tests

Sample	Irradiance (kW/m^2)	TTI (s)	TTE (s)	Mass (g)	Mass loss (g)	Residue (%)	THR (MJ/m^2)	PHRR (kW/m2)	COY (Kg/kg)
PP	50	29	325	65.6	65.6	0.0	277.4	2400	0.0344
SW30	50	14	412	65.7	55.1	16.1	192.6	689	0.0285

TTI: Time to Ignition; TTE: Time to Extinguish; THR: Total Heat Released; PHRR: Peak Heat Release Rate; COY: CO yield (average)

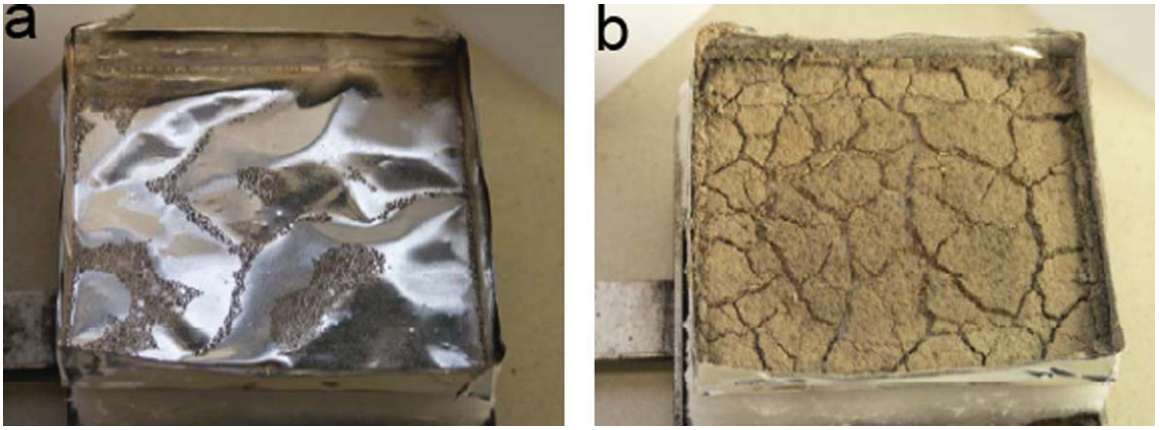

Figure 7 Sample residual after cone calorimetric test: (a) Neat PP; (b) SW30. [Color figure can be viewed in the online issue, which is available at www.interscience.wiley.com.]

The authors sincerely wish to express their appreciation to Dr. Bernard Schartel of the Federal Institute for Materials Research and Testing (BAM), Berlin, for cone calorimetric analysis and valuable interpretation. They also thank Sabic and Clariant for providing materials.

Reference

1. Bodors, E.; Baley, C. Mater Lett 2008, 62, 2143.
2. Mydul, M. A.; Toufiq, A.; Monimul, H. Polym Plast Technol Eng 2009, 42, 110.
3. Sui, G.; Fuqua, M. A.; Ulven, C. A.; Zhong, W. H. Biosource Technol 2009, 100, 1246.
4. Joshi, S. V.; Drzal, L. T.; Mohanty, A. K.; Arora, S. Compos Part A 2004, 35, 371.
5. Alexandre, G.; Takanori, M.; Koichi, G.; Junji, O. Compos Part A 2007, 38, 1811.
6. Keener, T. J.; Stuart, R. K.; Brown, T. K. Compos Part A 2004, 35, 357.
7. Sgriccia, N.; Hawley, M. C. Compos Sci Technol 2007, 67, 1986.
8. Sreekumar, P. A.; Albert, P.; Unnikrishnan, G. J Appl Polym Sci 2008, 109, 1547.
9. Rizvi, G. M.; Park, C. B.; Guo, G. J Cell Plast 2008, 44, 125.
10. Marcia, A.; Silva, S.; Karen, K. G.; Fermoseli, M. J Appl Polym Sci 2009, 112, 3686.
11. Muenir, T.; Hasan, B.; Gerald, T. J Appl Polym Sci 2009, 112, 3095.
12. Shigha, A. S.; Vijay, K. T. Polym Plast Technol Eng 2009, 48, 201.
13. Varga, J.; Karger-Kocsis, J. Polymer 1995, 36, 4877.
14. Araujo, J. R.; Waldman, W. R.; De Paoli, M. A. Polym Degrad Stab 2008, 93, 1770.
15. Ryszard, K.; Maria, W. P. Polym Adv Technol 2008, 19, 446.
16. Yongli, M.; Xiaoya, C.; Qipeng, G. J Appl Polym Sci 1997, 64, 1267.
17. Liu, T.; Petermann, J. Polymer 2001, 42, 6453.
18. Liu, T.; Petermann, J.; He, C. Macromolecules 2001, 34, 4305.
19. Schartel, B.; Braun, U.; Schwarz, U.; Reinemann, S. Polymer 2003, 44, 6241.
20. Hassan, M. M.; Mueller, M.; Wagner, M. H. J Appl Polym Sci 2008, 109, 1242.
21. Nitz, H.; Reichert, P.; Roemling, H.; Muelhaupt, R. Macromol Mater Eng 2000, 276, 51.
22. Slawmomir, B.; Dominik, P.; Malgorzata, H. Polym Degrad Stab 2006, 91, 3339.
23. Wunderlich, B. Thermal Analysis; Academic Press: New York, 1990; p 418.
24. David, P. H.; Marie-Pierre, G.; Laborie, M. P. J Appl Polym Sci 2009, 111, 753.
25. Mehdi, T.; Robert, H. F.; John, C. H. J Appl Polym Sci 2006, 101, 4341.
26. Turi, E. A. Thermal Characterization of Polymeric Materials; Academic Press: New York, 1997; 2420.
27. Amash, A.; Zugenmaier, P. J Appl Polym Sci 1997, 63, 1143.
28. Nielsen, L. E.; Landel, R. F. Mechanical Properties of Polymers and Composites; Marcel Dekker: New York, 1994; p 557.
29. Rana, A. K.; Mandal, A.; Jacobson, R.; Rowell, R.; Banerjee, A. N. J Appl Polym Sci 1998, 69, 329.
30. Tajvidi, M.; Falk, R. H.; Ebrahimi, G. H. In Proceedings of the 2nd International Conference on Wood Mechanics, Stockholm, Sweden; 2003; p 25.